PCCP

Accepted Manuscript

ROYAL SOCIETY OF CHEMISTRY

www.rsc.org/pccp

High Coverage Adsorption and Co-Adsorption of CO and H_2 on Ru(0001) from DFT and Thermodynamics

*Peng Zhao,[a,b,c] Yurong He,[a,b,c] Dong-Bo Cao,[a,b] Xiaodong Wen,[a,b] Hongwei Xiang[a,b] Yong-Wang Li,[a,b] Jianguo Wang,[a] Haijun Jiao[a,d]**

a) State Key Laboratory of Coal Conversion, Institute of Coal Chemistry, Chinese Academy of Sciences, Taiyuan, 030001, China; b) National Energy Center for Coal to Liquids, Synfuels China Co., Ltd, Huairou District, Beijing, 101400, China; c) University of Chinese Academy of Sciences, No.19A Yuquan Road, Beijing, 100049, PR China; d) Leibniz-Institut für Katalyse e.V. an der Universität Rostock, Albert-Einstein Strasse 29a, 18059 Rostock, Germany. E-mail: haijun.jiao@catalysis.de

Abstract

The adsorption and co-adsorption of CO and H_2 at different coverage on *p*(4×4) Ru(0001) have been computed using periodic density functional theory (GGA-RPBE) and atomistic thermodynamics. Only molecular CO adsorption is possible and the saturation coverage is 0.75 ML (n_{CO} = 12) with CO molecules co-adsorbed at different sites and has a hexagonal adsorption pattern as found by low energy electron diffraction. Only dissociative H_2 adsorption is possible and the saturation coverage is 1 ML (n_H = 16) with H atoms at face-centered cubic sites. The computed CO and H_2 desorption patterns and temperatures agree reasonably with the experiments at ultrahigh vacuum conditions. For CO and H_2 co-adsorption (nCO+$m$$H_2$; n = 1-6 and m= 7, 6, 5, 5, 3, 1), CO pre-coverage affects H adsorption strongly, and each pre-adsorbed CO molecule blocks 2H adsorption sites and H_2 does not adsorb on surface with CO pre-coverage larger than 0.44 ML (n_{CO} = 7); all these are in full agreement with the experiments at ultrahigh vacuum condition. Our results provide the basis for exploring the mechanisms of catalytic conversion of synthesis gas.

Keywords: Adsorption, Co-adsorption, CO, H_2, Ruthenium, DFT, Atomistic thermodynamics, Coverage

1. Introduction

The adsorption of CO as well as the co-adsorption of CO and H_2 on heterogeneous catalysts are associated with many important industrial processes, such as water-gas shift reaction for hydrogen production,[1] alcohols synthesis from CO hydrogenation,[2,3] and Fischer-Tropsch synthesis (FTS)[4] in converting synthesis gas ($CO+H_2$) into value-added chemicals and fuels.[5] Among all FTS active catalysts, Ru-based catalysts are most active as well as tolerant to water or other oxygen-containing species;[6] and this is of particular importance for the conversion of synthesis gas generated from biomass.[7]

In heterogeneous catalysis surface coverage is of paramount importance and coverage significantly influences not only binding energies of adsorbed species but also reaction mechanisms. On Ru-based catalysts, density functional theory (DFT) studies reveal direct CO dissociation on high-index surfaces at low coverage,[8,9] while H-assisted CO dissociation on low-index surfaces at high coverage.[10] Since catalysis on supported metal clusters often occurs at condition of adsorbates near saturation coverages, low-index Ru surfaces, e.g.; Ru(0001), may be more reactive. This is consistent with the catalytic activity of Ru particle sizes in FTS, i.e.; for particle size less than 10 nm, turnover frequency of CO consumption increases strongly as particle size increases, reaching a constant value for particle size larger than 10 nm,[11] indicating that low-index Ru surfaces, prevalent in large clusters,[12] are more effective.

Under ultra-high vacuum (UHV) condition CO is molecularly adsorbed on Ru(0001), and the coverage is about 0.66 monolayer (ML) at 300 K.[13,14] At low coverage, CO adsorption energy estimated by CO thermal desorption on Ru(0001) is −1.66 eV.[15] With the increase of coverage, C-O stretching frequency measured by infrared (IR) spectroscopy shifts continuously from 1984 to 2080 cm^{-1} at 100 K,[16] or from 1984 to 2061 cm^{-1} at 200 K,[17] suggesting that CO adsorbs exclusively on top sites on Ru(0001) up to high coverage. At 0.22 ML initial coverage, temperature programmed desorption (TPD) shows a single desorption peak at 490 K.[18] At 0.43 ML initial coverage, TPD shows a second desorption peak at 416 K, while at higher coverage (0.54 ML), a new peak is observed at about 370 K.[15] It is found that CO adsorption pattern depends on coverage, in turn, on temperature and pressure. At $\theta_{CO} \leq 1/3$ ML, both low energy electron diffraction (LEED)[19] and scanning tunneling microscopy (STM)[20] study showed a $(\sqrt{3}\times\sqrt{3})R30°$ adsorption pattern on Ru(0001). At $\theta_{CO} > 1/3$ ML, the adsorbed CO molecules at top sites tend to tilt to relieve the repulsive interactions.[20,21] At $\theta_{CO} = 3/4$ ML, which is almost the highest coverage reported in experiment, a hexagonal adsorption pattern has been observed by LEED.[22]

Besides the extensive experimental studies, there are computational investigations into CO adsorption on Ru(0001) for studying the influence of coverage and co-adsorbates.[23] Ciobica *et al.*,[24] calculated CO adsorption on Ru(0001) at 0.11, 0.25 and 0.33 ML coverage, and found that hexagonal cubic packed (hcp) and top sites have the same CO adsorption energy at 0.11 ML (−1.93 eV) and 0.25 ML (−1.83 eV), while at 0.33 ML, top site adsorption becomes more stable (−1.96 eV) than those of hcp, face-centered cubic (fcc) and bridge sites (−1.83, −1.76 and −1.72 eV, respectively), and forms a $(\sqrt{3}\times\sqrt{3})R30°$ adsorption pattern. McEwen *et al.*,[25] computed two CO adsorption models on Ru(0001); the first one with CO adsorbed upright on top and hollow sites and the second one with CO adsorbed tilted on top sites; and found that the second model is more consistent with the experiment on the basis of the IR results. Loveless *et al.*,[10] studied CO adsorption on Ru(0001) in a model just like the second one, and the calculated saturation coverage is about 0.9 ML, which is higher than the experimentally estimated saturation coverage (0.66 ML) under UHV condition at 300 K.[14] In addition, crystal orbital overlap population (COOP) was used to elucidate changes in the C-O and C-Ru distances up on coverage variation.[26]

In contrast to CO, H_2 adsorption is dissociative on Ru(0001) and the saturation fractional coverage is one adatom per Ru(0001) unit cell.[24,27,28] It is found that the adsorbed H atoms prefer 3-fold fcc sites instead of top, bridge or 3-fold hcp sites; and a 1:1 H/Ru ratio on the surface is favored. TPD shows a single H_2 desorption peak at around 390 K at low exposure; and a second H_2 desorption peak at about 330 K at high exposure.[29] According to the temperature dependent experiments at very low pressure,[30-32] increasing the temperature decreases H_2 coverage value, i.e.; 0.95 ML at 230 K, 0.78 ML at 250 K and 0.67 ML at 270 K. Ciobica *et al.*,[24] calculat-

ed H adsorption on Ru(0001) at 25-300% coverage and found that at 25% coverage adsorption at fcc site is more favorable (−0.55 eV) than at hcp, bridge and top sites (−0.52, −0.42 and −0.09 eV, respectively). At high coverage ($1/2 \le \theta_H \le 1$ ML), Rosal *et al.*,[32] found that the most favorable configurations are those having all H atoms occupying fcc sites.

Considering the influence of adsorbates on the dynamics of adsorption and dissociation of other species from gas phase, the co-adsorption of CO and H on Ru(0001) has also been studied. Ciobica *et al*.,[24] discussed the co-adsorption of H and CO on Ru(0001), and found that the lateral H and CO interaction is repulsive, as well as H and CO adsorption prefer to form islands rather than mixed structures. In addition, CO adsorption is slightly influenced by H co-adsorption, except at 1 ML pre-adsorbed H atoms, while H adsorption is strongly affected by CO co-adsorption. Kleyn *et al*.,[33] studied the influence of pre-adsorbed CO on D_2 dissociative adsorption on Ru(0001) by molecular-beam techniques and found that D_2 dissociation has CO-induced barrier in CO vicinity. At high CO coverage, D_2 dissociation occurs via penetration of the CO-induced barrier. Groot et al.,[34] studied hydrogen dissociation on a 1/3 ML CO-pre-covered Ru(0001) surface by means of six-dimensional quasi-classical and quantum dynamics. They found that both energy and rovibrational distributions of the molecular beam influence the reactivity, with the largest effect being caused by energy distribution. Diemant *et al*.,[35] investigated the combined interaction of D_2 and CO on Ru(0001) by TPD and IR spectroscopy, and obtained the composition and coverage of the adlayer formed under pressure and temperature relevant for operating low temperature fuel cells. They found that the amount of adsorbed D decreases steadily with increasing CO pre-coverage, and each CO molecule blocks on average 2 D adsorption sites for small to intermediate CO pre-coverage ($\theta_{CO} \le 1/3$ ML).

Most of the DFT studies about synthesis gas adsorption on Ru(0001) do not consider the influence of the reaction condition such as pressure, temperature and CO/H_2 ratio, although pressure and temperature are found to affect the adsorption configuration and coverage strongly.[14] In this work, we systematically investigated the stable coverage of CO and synthesis gas on Ru(0001) by using larger model and different methods under the consideration of temperature and pressure on the basis of *ab initio* atomistic thermodynamics.[36,37] Our computed results represent a first step in the exploration of the catalytic conversion of synthesis gas, and can be validated via direct comparison with the available experimental data.

2. Computational Details

2.1 Methods: All calculations were performed using the plane-wave based DFT method implemented in the Vienna Ab Initio Simulation Package (VASP).[38,39] The electron-ion interaction was described with the projector augmented wave (PAW) method.[40,41] Firstly, we used the generalized gradient approximation and the Perdew-Burke-Ernzerhof functional (GGA-PBE)[42] to describe the exchange and correlation energies for all systems. At PBE/PAW, CO adsorption prefers at both top and hcp sites (−1.92 and −1.94 eV, respectively); and this does not agree with the experimentally observed top site adsorption at low coverage. Then we used the revised Perdew-Burke-Ernzerhof functional (GGA-RPBE[43,44]) to describe the exchange and correlation energies for CO adsorption at different coverage; and it is found that RPBE/PAW not only predicts the more preferred top adsorption site but also perfectly reproduces the estimated CO adsorption energy. As a result, we carried RPBE single-point energy calculation on the PBE optimized structure; and the computed CO adsorption energy is practically the same as found from RPBE optimization. In our calculations, all adsorption structures are obtained from PBE optimization, while all energies are obtained from RPBE single-point energy calculations on the PBE structures. Despite of the excellent agreement in CO adsorption energy between experiment and RPBE computation, we are interested in the long-range dispersion corrections for van der Waals interaction. In our calculations we used the Grimme GGA-type functional (PBE-D3).[45] We found that PBE and PBE-D3 optimizations give practically the same adsorption configurations and geometries for 10CO and 14CO molecules (Figure S2 in **ESI**). However, it is found that such dispersion correction overestimates the CO adsorption strongly, i.e.; -2.20 vs. -1.92 eV by using PBE and -2.41 vs. -1.64 eV by using RPBE. All these results are listed in Table 1 as discussed below. We also found that dispersion correction overestimates the adsorption energy of H_2O on several iron surfaces.[46,47,48] However,

for the adsorption of H_2O and H_2 on the Cu(111) surface, the computed adsorption energies are in excellent agreement with the available experimental data.[49] In our computations, an energy cut-off of 400 eV and a second-order Methfessel-Paxton[50] electron smearing with σ = 0.2 eV were used to ensure accurate energies with errors due to smearing of less than 1 meV per unit cell. The vacuum layer between periodically repeated slabs was set as 15 Å to avoid interactions among slabs. To locate the transition sates of CO and H_2 dissociation on Ru(0001), the nudged elastic band (NEB)[51] method was applied and the stretching frequencies were analyzed to characterize transition state with only one imaginary frequency.

The adsorption energy [*E*(CO/ads)] of one CO molecule is defined as *E*(CO/ads) = *E*(CO/slab) – [*E*(slab] + *E*(CO)], where *E*(CO/slab) is the total energy of the slab with one CO, *E*(slab) is the total energy of the bare slab and *E*(CO) is the total energy of a free CO molecule in gas phase. The adsorption energy [*E*(H_2/ads/*n*CO-slab)] of one H_2 molecule on *n*CO pre-covered Ru(0001) surface is defined as *E*(H_2/ads/*n*CO-slab) = *E*(H_2/*n*CO-slab) – [*E*(*n*CO-slab) + *E*(H_2)], where *E*(H_2/*n*CO-slab) is the total energy of the slab with *n*CO and one H_2, *E*(*n*CO-slab) is the total energy of the slab with *n*CO, and *E*(H_2) is the total energy of a free H_2 molecule in gas phase. The more negative the E_{ads}, the stronger the adsorption. The dissociation barrier (E_a) and reaction energy (E_r) are defined as $E_a = E_{TS} - E_{IS}$ and $E_r = E_{FS} - E_{IS}$, where E_{IS}, E_{TS}, and E_{FS} are the energies of the corresponding initial state (IS), transition state (TS) and the final state (FS).

2.2 Models: Calculation of the Ru bulk crystal structure with a γ-centered k-point mesh of 3×3×1 gives lattice parameters (*a* = *b* = 2.731 Å and *c* = 4.310 Å) in good agreement with the experiments (*a* = *b* = 2.751 Å and *c* = 4.282 Å).[52] For studying CO adsorption on Ru(0001), we used the larger *p*(4×4) surface model with four atomic layers, where the top two layers including adsorbates were allowed to relax, and the bottom two layers are fixed in their bulk position.

2.3 Thermodynamics: As an efficient tool to extend the result of DFT to a more relevant temperature and pressure range, ab initio atomistic thermodynamics has been extensively and effectively applied in many systems.[53-57] According to our previous studies for CO adsorption;[58-61] we took CO adsorption on Ru(0001) surface: Ru + CO(g) → CO/Ru as an example; and the change of Gibbs free energy (ΔG) for this reaction can be described as Eq. 1.

$$\Delta G_{Ru}^{(0001)}\left(T,p,n_{CO}\right)=G\left[Ru\left(0001\right)/\left\{nCO\right\}\right]-G\left[Ru\left(0001\right)\right]-G_{gas}\left(CO\right) \quad (1)$$

In this formula, *G*[Ru(0001)/{*nCO*}] is the Gibbs free energy of the Ru(0001) surface with n CO molecules, and *G*[Ru(0001)] is the Gibbs free energy of the clean Ru(0001) surface. Because of the large mass differences, the contribution of vibration to the solid surfaces is negligible. Therefore, we apply the DFT calculated total energy (E_{total}) to substitute the Gibbs free energies of the solid surfaces. The $G_{gas}(CO)$ term is equal to $n_{CO}\mu_{CO}(T,p)$, and the CO chemical potential can be expressed as

$$\mu_{CO}\left(T,p\right)=E_{CO}^{total}+\tilde{\mu}_{CO}\left(T,p^0\right)+k_BT\ln\left(p_{CO}/p^0\right)$$

At 0 K, the CO chemical potential can be regarded as the total energy of the isolated CO molecule (including zero point energy) which can be calculated directly with VASP. The $\tilde{\mu}_{CO}\left(T,p^0\right)$ term is the chemical potential at different temperatures, which can be found in thermodynamic tables. The last term of this formula is the contribution of temperature and CO partial pressure to the CO chemical potential. Therefore, Eq. 1 can be rewritten as

$$\Delta G_{Ru}^{(0001)}\left(T,p,n_{CO}\right)=E\left[Ru\left(0001\right)/\left\{nCO\right\}\right]-E\left[Ru\left(0001\right)\right]-nE_{CO}^{total}-n\tilde{\mu}_{CO}\left(T,p^0\right)-nk_BT\ln\left(p_{CO}/p^0\right) \quad (2)$$

In this respect, we can plot *G*[Ru(0001)/{*nCO*}] as a function of T and p_{CO}. Analogously, the change of Gibbs free energy (ΔG) for the co-adsorption of CO and H_2 on Ru(0001) can be expressed as Eq. 3.

$$\begin{aligned}\Delta G_{Ru}^{(0001)}\left(T,p_{CO},p_{H_2},nCO,mH_2\right)&=E\left[Ru(0001)/\left\{nCO,mH_2\right\}\right]-E\left[Ru(0001)\right]\\&-nE_{CO}^{total}-n\tilde{\mu}_{CO}\left(T,p^0\right)-nk_BT\ln\left(p_{CO}/p^0\right)-mE_{H_2}^{total}-m\tilde{\mu}_{H_2}\left(T,p^0\right)-mk_BT\ln\left(p_{H_2}/p^0\right)\end{aligned} \quad (3)$$

In this respect, we can plot *G*[Ru(0001)/{*nCO+mH*$_2$}] as a function of T, p_{CO} and p_{H2}.

3 Results and discussions

(a) One CO adsorption: There are four adsorption sites on Ru(0001); top (**t**), bridge (**b**) as well as three-fold hcp hollow (**h**) and fcc hollow (**f**) sites (Figure 1). For one CO on Ru(0001) (1/16 ML), CO adsorption energy is −1.65 eV for **t** site, −1.58 eV for **h** site, −1.47 eV for **f** and **b** sites by RPBE (Table 1). It is also clearly shown that the computed CO adsorption energies from RPBE optimization are nearly the same as obtained from RPBE single-point calculation on the PBE structure. The same trend is also found at 1/4 and 1/2 ML. In our following discussion comparison, we used the RPBE computed single-point energies. It is noted that CO adsorption energy on Ru(0001) differs strongly from methods, at 1/4 ML for example, −1.49 eV by B3LYP,[26] −1.64 eV by RPBE/PAW, and −1.83 eV by PW91/USSP.[24] Our RPBE value (−1.65 eV) is consistent with the experimental value (−1.66 eV) estimated from CO thermal desorption on Ru(0001) at low coverage.[15] In addition, only RPBE can predict top adsorption site as most favorable at low coverage, which is consistent with the result of IR study.[17] However, dispersion correction for van der Waals interaction (RPBE-D3) overestimates the CO adsorption by 0.77 eV, and therefore we used the pure RPBE energies for our comparison and discussion (Table 1).

(Figure 1 and Table 1)

In order to make sure that CO adsorbs non-dissociatively, we computed the more competitive CO dissociation pathway proved by Ciobica *et al*.8 The energy of CO desorption at hcp site (1.58 eV, Table 1) is lower than CO dissociation barrier (2.25 eV); and CO dissociation is endothermic by 0.38 eV. This indicates a preference for CO (θ_{CO}= 1/16 ML) desorption over dissociation. For CO dissociation on hcp site (Table 2), it is noted that the barriers and the reaction energies are not dependent on the methods;[8,62,63] and the corrections from zero-point energies have negligible effects on CO dissociation barrier and reaction energy.

(Table 2)

(b) High Coverage CO adsorption: We calculated all possible CO adsorption configurations on Ru(0001) at different coverage to find the most stable configuration at individual coverage. In order to get the saturation coverage, we used the stepwise adsorption energy, $\Delta E_{ads} = E_{(CO)n+1/slab} - [E_{(CO)n/slab} + E_{CO}]$, where a positive ΔE_{ads} for n+1 adsorbed CO molecules indicates the saturation adsorption with *n*CO molecules. The structures and energies (ΔE_{ads}) of the most stable adsorption sites for stepwise CO adsorption are given in Figure 2. The PBE values are given in ESI for comparison. To judge top, bridge and three fold adsorption sites, we used the C-Ru distances as the criterion, i.e.; top site has only one C-Ru distance; bridge site has two close C-Ru distances and three-fold site has three close C-Ru distances.

(Figure 2)

The first four adsorbed CO molecules (n_{CO} = 1-4) are located on top sites and have very close stepwise adsorption energies (−1.64, −1.63, −1.63 and −1.64 eV), indicating their negligible lateral repulsive interaction. At n_{CO} = 5-7, lateral repulsive interaction becomes significant; and all adsorbed CO molecules are tilted on top sites and the stepwise adsorption energies are in a close range (−1.37, −1.43 and −1.43 eV). At n_{CO} = 8, the adsorbed CO molecules are tilted on top sites, forming the $(CO)_n$-Linear configuration discovered by LT-STM,[20] but the stepwise adsorption energy is lower (−1.15 eV). At n_{CO} = 9 and 10, all adsorbed CO molecules are tilted on the top site. At n_{CO} = 11, there are three CO molecules tilted at top sites, six CO molecules at bridge sites as well as one CO molecule at hcp and one CO molecule at fcc sites. At n_{CO} = 12, there are four CO molecules at top sites, four CO molecules at hcp and four CO molecules at fcc sites. Despite these different adsorption sites, the stepwise adsorption energies for n_{CO} = 9-12 are close (−0.86, −0.79, −0.91 and −0.84 eV). At n_{CO}=13, there are seven CO molecules tilted at top sites, five CO molecules at bridge sites and one molecule at hcp site; and the stepwise adsorption energy becomes slightly positive (0.03 eV); and the saturation coverage should have twelve CO molecules (θ_{CO} = 0.75 ML), and this is more close to the experimental one (0.68 and 0.66 ML) at 200 K[17] and 300 K,[14] than the computed 0.9 ML by Loveless *et al.*[10] The adsorption configuration at saturation coverage is consistent with the "hexagonal" pattern observed by LEED at same coverage (0.75ML),[22] which is denser than the other "hexagonal" structure observed by STM at lower coverage (0.58 ML).[20] Such small stepwise adsorption energy at n_{CO} = 13 shows the possibility of higher coverage at

high pressure. At n_{CO} = 14-16, the stepwise adsorption energies are positive by 1.04, 1.14 and 0.18 eV. At n_{CO} = 14, there are six CO molecules tilted at top sites, six CO molecules at bridge sites as well as one CO molecule at hcp and one CO molecule at fcc sites. At n_{CO} = 15 and 16, only top CO adsorption has been found; and the 1 ML coverage has sixteen adsorbed CO molecules at top sites.

As shown in Table 3, the C-O stretching frequency (ν_{CO}, cm^{-1}) are systematically underestimated at all coverage of CO adsorbed on top sites (n = 1-10) by using PBE compared with the experimental values.[17] However, it is noted that the difference in average C-O stretching frequency between one and ten CO molecules is the same as that observed from experiment (60 cm^{-1}).

(Table 3)

(c) CO coverage on temperature and pressure: As referred to *ab initio* atomistic thermodynamics, we used ΔG as a criterion to test the stability of *n*CO adsorbed system under different conditions, and the more negative the ΔG, the more stable the adsorbed structure. On the basis of the calculated total energies of different stable structures and CO chemical potentials under different conditions, we plotted the equilibrium phase diagram of stable CO coverage as functions of temperature and CO partial pressure (Figure 3); where there are six regions and each region shows the possibility for getting stable CO coverage within the range of temperature or partial pressure. The first region shows the coverage of 0.81 ML (n_{CO} = 13), which is only stable at very low temperature (< 50 K). The second region shows the coverage of 0.75 ML (n_{CO} = 12), which is quite stable at wide temperature. The third, fourth and fifth regions show the coverage of 0.50, 0.43 and 0.25 ML (n_{CO} = 8, 7 and 4, respectively), respectively, and they have comparatively narrow temperature ranges. The last region is the clean surface and free from CO molecules.

(Figure 3)

On the basis of this phase diagram, it is possible to compare our results with the available experimental data obtained within a temperature range at fixed CO partial pressure (p_{CO}). Under UHV condition (5×10^{-11} mbar),[15,18] we plotted the change of Gibbs free energy as function of temperature and found four cross points among those lines (Figure 4), and each point indicates the equilibrium of coverage change at the corresponding temperature. The first CO desorption starts from n_{CO} = 12 to 8 at 220-240 K (0.75 to 0.50 ML); the second CO desorption starts from n_{CO} = 8 to 7 at 270-280 K (0.50 to 0.43 ML); and the third CO desorption starts from n_{CO} = 7 to 4 at 340-360 K (0.43 to 0.25 ML); and the final CO desorption starts from 0.25 ML to become a clean surface at 390-410 K. Compared with the experimental TPD results (heating rate 5 K/s) of 370 K at 0.54 ML, 416 K at 0.43 ML and 490 K at 0.22 ML,[15,18] our computed desorption temperatures are about 90-70 K lower. One reason for this disagreement might be neglected entropy effect in Gibbs free energy.[64] However, it is noted that for CO desorption temperature and thermodynamics on iron surfaces well agreements between theory and experiment have been found by using the same methodology.[59] Since each experimental TPD desorption peak represents a temperature range; our computed desorption temperatures fit into the down limit. These agreements provide the information for predicting CO desorption properties on the catalyst surfaces.

(Figure 4)

(d) High coverage H_2 adsorption: As reported previously,[24,28] we also found that the adsorbed H atom prefers fcc site (-0.46 eV), while adsorption on hcp (–0.42 eV) site is slightly higher in energy. It is noted that our H computed adsorption energy at fcc site is lower than that (–0.55 eV) reported by Ciobica et al,[24] by using different model and method. For one H_2 adsorption, H_2 is molecularly adsorbed at top site, while dissociatively adsorbed at bridge, hcp and fcc sites. For dissociation of molecularly adsorbed H_2 at top, the dissociating H-H distance in the transition state is 1.153 Å, and the computed dissociation barrier is 0.03 eV, and the dissociation energy is –0.65 eV. The adsorption energy of 2H at the most favorable fcc sites is –0.91 eV. All these indicate the preferred dissociative adsorption of H_2 on Ru(0001). We therefore computed H_2 adsorption at high coverage (Figure 5).

(**Figure 5**)

There are four groups for H_2 adsorption on the basis of the computed stepwise dissociative adsorption energies. Each group has

two dissociatively adsorbed H_2 molecules, and the stepwise dissociative adsorption energies are the same or nearly the same. With the increase of H_2 coverage, the stepwise dissociative adsorption energies decrease from –0.91 eV for the first two H_2 molecules to –0.88 and –0.86 eV for the second two H_2 molecules as well as to –0.67 eV for third two H_2 molecules and finally to –0.61 eV for the last two H_2 molecules, indicating the increase of the lateral repulsive interaction. In all these adsorption configurations, the adsorbed H atoms are located at fcc sites; and this is consistent with the results of $1/2 \le \theta_H \le 1$ ML by Rosal *et al.*[32]

At $\theta_H > 1$ ML, molecular H_2 adsorption becomes possible. The ninth H_2 molecule is located at the top sites, and the stepwise adsorption energy increases rapidly and becomes positive (0.72 eV), indicating very strong lateral repulsive interaction. Therefore, the saturation coverage is 1 ML, which is consistent with the result of Lindroos et al,[28] while disagrees with the results of Ciobica *et al.,*[24] where they reported 25-300% H coverage on Ru(0001) on the basis of average adsorption energy.

On the basis of the computed Gibbs free energies as a function of temperature under UHV condition (2.6×10^{-13} atm) we calculated H_2 desorption temperatures on Ru(0001) and found four transition temperatures (Figure 6), i.e.; at 255K from 1 and 0.75 ML, at 270 K from 0.75 and 0.5 ML and at 320K from 0.5 and 0.25 ML as well as finally at 330K from 0.25 to 0 ML (at 2.6×10^{-13} atm, the transition temperature is 255, 270, 320 and 330K, respectively). This is in agreement with the results (270, 285, 310, and 330K) predicted by Rosal.[32] Our results are also consistent with the temperature dependent experiments (0.95 ML at 230K and 0.78 ML at 250K) at very low pressure.[31,32,32] Considering the small deviation (10-20K) between the first two as well as the last two transition temperatures, there are two desorption peaks (Figure 6). The first H_2 desorption starts from n_{H2} = 8 to 4 (1.0 to 0.50 ML) at 240-265K; the second H_2 desorption starts from n_{H2} = 4 to 0 (0.50 to 0 ML) at 320-330K (at 1×10^{-10} mbar, the desorption temperature is in the range of 230-250 and 310-320K, respectively). Although our predicted desorption temperatures are about 90-70 K lower than the experimental TPD results[29] (330 and 390 K), the temperature difference between two peaks found around 70 K is in very good agreement with experimental results.

(**Figure 6**)

(e) Co-adsorption of H_2 and CO: Apart from the individual adsorption of CO and H_2, we computed their co-adsorption in different surface ratios. Since CO adsorption energies are much stronger than those of H_2 in a wide range of coverage, we used the most stable CO adsorption configurations (Figure 2) as CO pre-covered surfaces, and calculated all possible H_2 adsorption configurations on nCO pre-covered Ru(0001) surface at different coverage for searching the most stable CO and H_2 co-adsorption configurations at individual coverage. The adsorption sites and energies (ΔE_{ads}) of the most stable adsorption configurations for stepwise H_2 adsorption are given in Table 4. The optimized geometries of these configurations are given in the ESI.

(Table 4)

For n_{CO} = 1-3, H_2 molecules prefer dissociative adsorption and all hydrogen atoms are located at fcc sites. On the basis of the computed stepwise adsorption energies, CO pre-covered surfaces can adsorb fourteen (1CO+14H), twelve (2CO+12H), and ten H atoms (3CO+10H); and the stepwise adsorption energy of the next H_2 is positive (0.18, 0.24, and 0.22 eV, respectively). These results are consistent with the experimental results,[35] i.e.; the amount of adsorbed D decreases steadily with increasing CO pre-coverage, and each CO molecule blocks on average 2 D adsorption sites at low CO pre-coverages ($\theta_{CO} \le 1/3$ ML). In addition, our results also are in reasonable agreement with the UHV experiment. For example, the computed CO+H co-adsorption coverage is 0.06+0.88 ML for 1CO+14H; 0.13+0.75 ML for 2CO+12H, and 0.19+0.63 ML for 3CO+10H; and the experimentally determined CO+D co-adsorption coverage is 0.04+0.81, 0.11+0.74, and 0.21+0.57 ML, where the surface was exposed to a dose of 45 L D_2 after pre-adsorption of increasing amounts of CO.[35]

For n_{CO} = 4-6, the pre-adsorbed CO molecules affect obviously the adsorption energies and stable coverage of H atoms. On the basis of the computed stepwise adsorption energies, the 4CO pre-covered surface can adsorb ten H atoms (4CO+10H), which are

located at fcc and hcp sites. The stepwise adsorption energy of the first five H_2 is –0.64, –0.63, –0.45, –0.47 and –0.26 eV, respectively; and the next H_2 adsorption has positive adsorption energy (0.31 eV). On the 5CO pre-covered surface, the first three H_2 molecules prefer dissociative adsorption (5CO+6H), and the stepwise adsorption energy is –0.65, –0.60, and –0.51eV, respectively; and the stepwise adsorption energy of the fourth and fifth H_2 molecules is 0.00 and 0.41 eV, respectively. On the 6CO pre-covered surface, the first H_2 prefer dissociative adsorption (6CO+2H); and the stepwise adsorption energy of the second and third H_2 molecules is 0.09 and 0.06 eV, respectively. On 7CO and 8CO pre-covered surfaces, only molecular H_2 adsorption is possible; and the adsorption energies are positive, and it is therefore not possible to adsorb H_2 molecules with CO pre-coverage larger than 0.44 ML (n_{CO} = 7).

With the increase of CO pre-coverage, the H coverage decreases steadily; and at 0.44 ML CO pre-coverage the surface is free from H_2. Our results are also in agreement with the experiment,[33] which shows that the dissociative adsorption probability of D_2 on *n*CO pre-covered Ru(0001) decreases linearly with increasing θ_{CO}, and down to almost zero when θ_{CO} = 0.44 ML.

On the basis of these results, it is possible to estimate H_2 desorption from CO pre-covered surfaces. On the clean surface, the computed H_2 desorption temperature is about 250 and 320 K; while at about 330 K, the surface is covered by 7CO (0.44 ML, n_{CO} = 7) and cannot adsorb H_2. Since the first H_2 dissociative adsorption energies on 4CO, 5CO and 6CO pre-covered surfaces are close to the stepwise dissociative adsorption energies of $5H_2$ to 8 H_2 on the clean surface (Figure 5), the corresponding H_2 desorption temperatures should be around 250 K on the CO pre-covered surfaces (n_{CO} = 4-6). Since the first H_2 dissociative adsorption energies on 1CO, 2CO and 3CO pre-covered surfaces are close to the stepwise dissociative adsorption energies of $1H_2$ to 4 H_2 on the clean surface (Figure 5), the corresponding H_2 desorption temperatures should be around 320 K on the CO pre-covered surfaces (n_{CO} = 1-3).

4. Conclusion

In combination of periodic density functional theory and atomistic thermodynamics, the adsorption and desorption as well as co-adsorption of CO and H_2 on the Ru(0001) surface have been computed at different coverage.

On the basis of the observed IR spectroscopic information and the estimated CO adsorption energies from experiments it is found that the revised-PBE method (RPBE) not only gives the preferred adsorption configuration at top site and but also reproduces the adsorption energy, while the PBE method favors the wrong adsorption configuration at the hexagonal cubic packed site and overestimates adsorption strength. These verify the RPBE method to be reasonable for CO adsorption on Ru surfaces. It is noted that dispersion correction for van der Waals interaction (RPBE-D3) overestimates the CO adsorption strength strongly.

Within the framework of a *p*(4×4) surface size (16 surface Ru atoms), the computed CO dissociation barrier is much higher than CO adsorption energy, and therefore only molecular CO adsorption is possible. The most stable CO adsorption configuration changes from right up to tilted on top sites from the lowest up to 0.63 ML (n_{CO} = 10). At saturation coverage (0.75 ML, n_{CO}= 12), the most stable adsorption configuration has the coexistence of top (4CO), hcp (4CO), and fcc (4CO) adsorption sites and they form a high symmetrical and periodic hexagonal pattern as found by low energy electron diffraction. It is noted that the PBE method underestimates CO stretching frequencies, but the shifts of the CO stretching frequencies upon the increase of CO agree very well between theory and experiment. It is also noted that the computed CO adsorption pattern agrees with the experiments under ultrahigh vacuum conditions, but CO desorption temperatures are underestimated quantitatively by 90-70K. Since the each experimental TPD desorption peak represents a temperature range and our computed desorption temperatures fit into the down limit.

In contrast to CO, only dissociative H_2 adsorption is found and the adsorbed H atoms are located at the face-centered cubic sites. The saturation is 1 ML (n_H = 16). Although the computed H_2 adsorption pattern agrees with the experiments under ultrahigh vacuum conditions, H_2 desorption temperatures are underestimated quantitatively by 90-70K and the temperature difference between two desorption peaks of around 70 K is in very good agreement with experimental results.

For CO and H_2 co-adsorption (*n*CO+*m*H_2), the most stable adsorption configuration has the formula of *n* = 1-6 and *m*= 7, 6, 5, 5, 3,

1. Due to the much stronger adsorption energy of CO over H_2, CO pre-coverage is found to affect H adsorption strongly. With the increase of CO pre-coverage, not only the number but also the strength of H_2 adsorption decrease. Each pre-adsorbed CO molecule can block 2H adsorption sites and H_2 does not adsorb on surface with CO pre-coverage larger than 0.44 ML (n_{CO} = 7); all these are in full agreement with the experiments about CO and D_2 co-adsorption at ultrahigh vacuum conditions. On the basis of the computed stepwise H_2 dissociative adsorption energies, it is expected that at high CO pre-coverage (n_{CO} = 4-6), H_2 desorption shifts to lower temperatures, while at low CO pre-coverage (n_{CO} = 1-3), H_2 desorption temperatures do not change.

The reasonable agreement between theory and experiment in the adsorption and co-adsorption of CO and H_2 on Ru(0001) surface validates our models and methods in one hand; in the other hand, our systematic study and detailed results provide the basis for understanding the initial stage of mutual influences of CO and H_2 co-adsorption and for exploring the mechanisms of catalytic conversion of synthesis gas.

Acknowledgment: This work was supported by the National Basic Research Program of China (no. 2011CB201406), the National Natural Science Foundation of China (no. 21273262, 21273266, and 21473229), the innovation foundation of Institute of Coal Chemistry, Chinese Academy of Sciences (no. Y4SC821981), and the Chinese Academy of Science and Synfuels CHINA. Co., Ltd.

Electronic Supplementary Information (ESI): Stepwise CO adsorption structures and energies (ΔE_{ads}) on Ru(0001) obtained from PBE functional (Figure S1); 10CO and 14CO adsorption structures and energies (ΔE_{ads}) on Ru(0001) using the PBE and PBE+D3 (Figure S2); stepwise H_2 adsorption structures and energies (ΔE_{ads}) on nCO pre-covered Ru(0001) (Figure S3); dependence of surface Gibbs free energy (ΔG) and H_2 on temperature at $p_{H2}/p^0 = 1\times10^{-13}$(Figure S4); and stepwise CO adsorption energies (E_{ads}, eV) including D3 corrections at different coverage (Table S1).

Figure 1: Schematic side (left) and top (right) views of the periodical model surface structures of Ru(0001) as well as possible adsorption sites: on-top (**t**), bridge (**b**), hcp hollow (**h**) and fcc hollow (**f**)

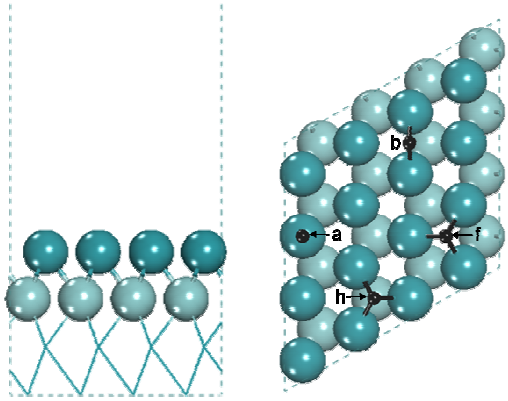

Figure 2: Stepwise CO adsorption structures and energies (ΔE_{ads}) on Ru(0001) (surface Ru/blue; C/black; O/red)

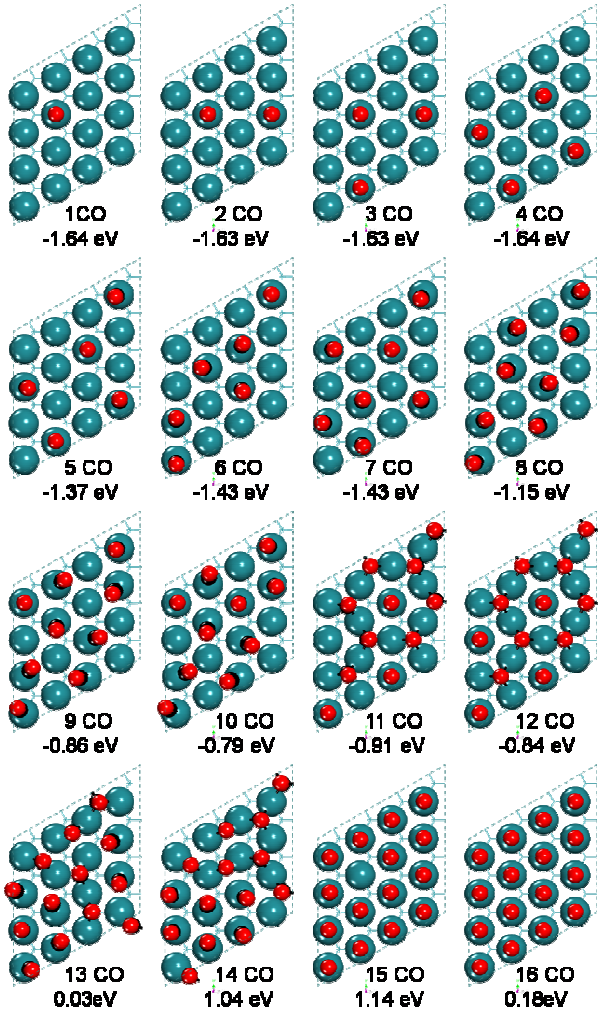

Figure 3: Equilibrium phase diagrams of stable CO coverage as a function of temperature and CO partial pressure ($\ln(p_{CO}/p^0)$)

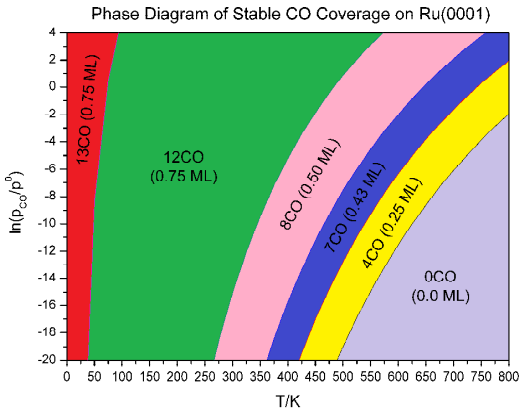

Figure 4. Dependence of surface Gibbs free energy (ΔG) and CO on temperature at $p_{CO}/p^0 = 5\times10^{-14}$

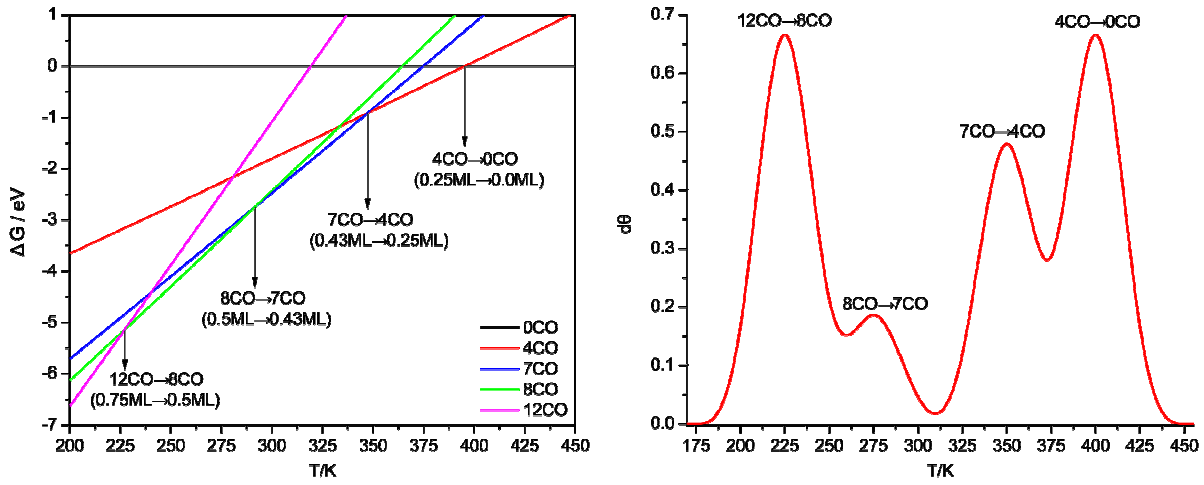

Figure 5: Stepwise H_2 adsorption structures and energies (ΔE_{ads}) on Ru(0001) (surface Ru/blue; H/yellow)

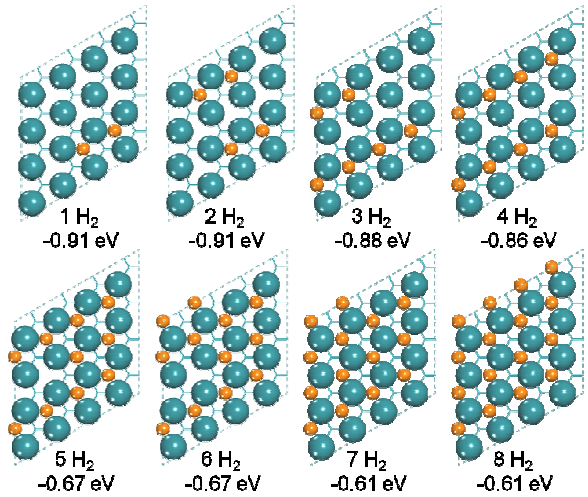

Figure 6: Dependence of surface Gibbs free energy (ΔG) and H_2 on temperature at $p_{H2}/p^0 = 2.6\times10^{-13}$

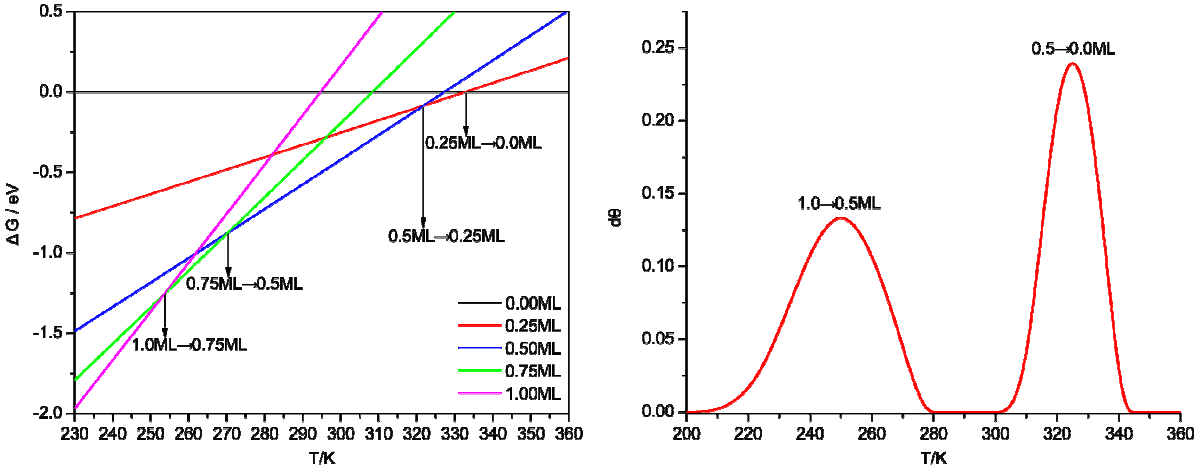

Table 1: CO adsorption energies (E_{ads}, eV) on Ru(0001) at different coverage using different methods, surface sizes and slab thicknesses (*m*L*n*R, *m* for total slab layers, and *n* for relaxed surface layers) at top (**t**), bridge (**b**), hcp (**h**) and fcc (**f**) sites

*Method and Size (m*L*n*R*)*	*Site*	E_{ads}
PBE/USPP [(4×4), 4L/2R]; 1/16 ML	**t**	-1.91
	h	-2.05
	f	-1.91
	b	-1.89
PBE/PAW [(4×4), 4L/2R]; 1/16 ML	**t**	-1.92 (2.20[b])
	h	-1.94
	f	-1.83
	b	-1.81
RPBE/PAW [(4×4), 4L/2R]; 1/16 ML	**t**	-1.65 (-1.64[a]) (2.41[c])
	h	-1.58 (-1.57[a])
	f	-1.47 (-1.46[a])
	b	-1.47 (-1.46[a])
PW91/USPP [(3×3), 2L/2R]; 1/9 ML	**t**	-1.93[24]
	h	-1.93[24]
RPBE/USPP [(3×3), 4L/2R]; 1/9 ML	**t**	-1.64[10]
B3LYP/6-311+G** [(3×3), 4L/2R]; 1/9 ML	**t**	-1.56[26]
RPBE/PAW [(4×4), 4L/2R]; 1/4 ML	**t**	-1.64 (-1.64[a]) (2.29[c])
	h	-1.52 (-1.52[a])
PW91/USPP [(2×2), 2L/2R]; 1/4 ML	**t**	-1.83[24]
	h	-1.82[24]
B3LYP/6-311+G** [(2×2), 3L/2R]; 1/4 ML	**t**	-1.49[26]
PBE/PAW [(4×4), 4L/2R]; 1/2 ML	**t**	-1.80 (2.12[b])
RPBE/PAW [(4×4), 4L/2R]; 1/2 ML	**t**	-1.49 (-1.49[a]) (2.28[c])
B3LYP/6-311+G** [(2×2), 3L/2R]; 1/2 ML	**t**	-1.44[26]

(a) Derived from RPBE single-point energy calculations on the PBE optimized structures in parenthesis. (b) Derived from D3 single-point energy calculations on the PBE optimized structures in parenthesis. (c) Derived from D3 single-point energy calculations on the RPBE optimized structures in parenthesis.

Table 2: CO dissociation barrier (E_a, eV) and dissociation energy (E_r, eV) on Ru(0001) using different methods, surface sizes and slab thicknesses (*m*L*n*R, *m* for the total slab layers, and *n* for the relaxed surface layers) at top (**t**), hcp (**h**) and fcc (**f**) sites

pathway	*m*L*n*R	*Method*	E_a	E_r
CO(**h**) → C(**h**) + O(**h**)	2×2 (2L2R)	PW91/USPP[8]	2.35	1.03
CO(**t**) → C(**h**) + O(**h**)	2×2 (2L2R)		3.41	1.04
CO(**h**) → C(**h**) + O(**f**)	2×2 (2L2R)		2.47	1.34
CO(**f**) → C(**f**) + O(**h**)	2×2 (2L2R)		3.30	1.57
CO(**h**) → C(**h**) + O(**h**)	3×3 (2L2R)		2.24	0.44
CO(**h**) → C(**h**) + O(**h**)	3×3 (4L1R)	PW91/USPP[62]	2.23	0.68
CO(**h**) → C(**h**) + O(**h**)	4×4 (4L2R)	PBE/PAW	2.13	0.21
CO(**h**) → C(**h**) + O(**h**)	4×4 (4L2R)	RPBE/PAW	2.25	0.38
CO(**h**) → C(**h**) + O(**h**)	4×4 (4L2R)	RPBE(ZPE)/PAW	2.17	0.39

Table 3: C-O stretching frequency (ν_{CO}, cm^{-1}) from DFT and IR in the CO/Ru(0001) system as a function of coverage (ML)

ML	ν_{CO} (PBE)	ML	ν_{CO} (200 K)[17]
0.06	1898	0.05	1990
0.13	1891-1904	0.13	2009
0.19	1889-1909	0.18	2012
0.25	1891-1917	0.26	2015
0.31	1887-1978	0.33	2022
0.38	1940-1991	0.37	2025
0.44	1948-2018	0.43	2035
0.5	1934-2026	0.48	2038
0.56	1926-2022	0.56	2040
0.63	1922-2031	0.61	2050

Table 4. Stepwise co-adsorption energies (eV) and adsorption sites (**f**, **h** and **b** for fcc, hcp, and bridge sites of dissociative adsorption, respectively, and **t** for top site of molecular adsorption) of mH_2 on the *n*CO pre-covered Ru(0001) surface

	1CO	2CO	3CO	4CO	5CO	6CO	7CO	8CO
$1H_2$	-0.91 [2**f**]	-0.93 [2**f**]	-0.87 [2**f**]	-0.64 [1**f**+1**h**]	-0.65 [2**f**]	-0.51 [1**f**+1**h**]	0.08 [1**t**]	0.11 [1**t**]
$2H_2$	-0.91 [4**f**]	-0.84 [4**f**]	-0.83 [4**f**]	-0.63 [3**f**+1**h**]	-0.60 [4**f**]	0.09 [1**f**+1**h**+1**t**]	0.08 [2**t**]	0.20 [2**t**]
$3H_2$	-0.86 [6**f**]	-0.81 [6**f**]	-0.78 [6**f**]	-0.45 [3**f**+3**h**]	-0.51 [6**f**]	0.06 [1**f**+1**h**+2**t**]	0.15 [3**t**]	0.31 [3**t**]
$4H_2$	-0.75 [8**f**]	-0.76 [8**f**]	-0.55 [8**f**]	-0.47 [4**f**+4**h**]	0.00 [6**f**+1**t**]			
$5H_2$	-0.68 [10**f**]	-0.70 [10**f**]	-0.28 [10**f**]	-0.26 [4**f**+6**h**]	0.41 [5**f**+5**h**]			
$6H_2$	-0.68 [12**f**]	-0.28 [12**f**]	0.22 [7**f**+5**h**]	0.31 [2**f**+5**h**+1**b**+2**t**]				
$7H_2$	-0.44 [14**f**]	0.24 [13**h**+1**b**]						
$8H_2$	0.18 [15**f**+1**b**]							

References

1 F. Boccuzzi, A. Chiorino, M. Manzoli, D. Andreeva and T. Tabakova, *J. Catal.*, 1999, **188**, 176-185.

2 R. G. Herman, *Catal. Today*, 2000, **55**, 233-245.

3 S. A. Hedrick, S. S. C. Chuang, A. Pant and A. G. Dastidar, *Catal. Today*, 2000, **55**, 247-257.

4 F. Fischer and H. Tropsch, *Brennstoff Chem.*, 1923, **4**, 276-285.

5 H. Schulz, *Appl. Catal.*, *A*, 1999, **186**, 3-12.

6 M. Benaissa, U. J. Jáuregui-Haza, I. Nikov, A. M. Wilhelm and H. Delmas, *Catal. Today*, 2003, **79-80**, 419-425.

7 D. A. Simonetti, J. Rass-Hansen, E. L. Kunkes, R. R. Soares and J. A. Dumesic, *J. A. Green Chem.*, 2007, **9**, 1073-1083.

8 I. M. Ciobica and R. A. van Santen, *J. Phys. Chem. B*, 2003, **107***,* 3808-3812.

9 S. Shetty, A. P. J. Jansen and R. A. van Santen, *J. Am. Chem. Soc.*, 2009, **131**, 12874-12875.

10 B. T. Loveless, C. Buda, M. Neurock and E. Iglesia, *J. Am. Chem. Soc.*, 2013, **135**, 6107-6121.

11 J. M. G. Carballo, J. Yang, A. Holmen, S. Garcia-Rodriguez, S. Rojas, M. Ojeda and J. L. G. Fierro, *J. Catal.*, 2011, **284**, 102-108.

12 R. V. Hardeveld and F. Hartog, *Surf. Sci.*, 1969, **15**, 189-230.

13 J. C. Fuggle, T. E. Madey, M. Steinkilberg and D. Menzel, *Surf. Sci.*, 1975, **52**, 521-541.

14 D. E. Starr and H. Bluhm, *Surf. Sci.*, 2013, **608**, 241-248.

15 H. Pfnür, P. Feulner and D. Menzel, *J. Chem. Phys.*, 1983, **79**, 4613-4623.

16 G. E. Thomas and W. H. Weinberg, *J. Chem. Phys.*, 1979, **70**, 1437-1439.

17 H. Pfnür, D. Menzel, F. M. Hoffmann, A. Ortega and A. M. Bradshaw, *Surf. Sci.*, 1980, **93**, 431-452.

18 S. Kneitz, J. Gemeinhardt and H. P. Steinrück, *Surf. Sci.*, 1999, **440**, 307-320.

19 T. E. Madey and D. Menzel, *J. Appl. Phys. Suppl.*, 1974, **2**, 229-235.

20 Q. W. Chen, J. Liu, X. Zhou, J. Shang, Y. J. Zhang, X. Shao, Y. F. Wang, J. L. Li, W. Chen, G. Q. Xu and K. Wu, *J. Phys. Chem. C*, 2015, **119**, 8626-8633.

21 P. Jakob, *J. Chem. Phys.*, 2015, **120**, 9286-9296.

22 J. P. Biberian and M. A. Van Hove, *Surf. Sci.*, 1984, **138**, 361-389.

23 J. L. C. Fajín, M. N. D. S. Cordeiro and J. R. B. Gomes, *Catalysts,* 2015, **5**, 3-17.

24 I. M. Ciobica, A. W. Kleyn and R. A. van Santen, *J. Phys. Chem. B*, 2003, **107***,* 164-172.

25 J. S. McEwen and A. Eichler, *J. Chem. Phys.*, 2007, **126**, 094701 (1-14).

26 N. Dimakis, N. E. Navarro, T. Mion and E. S. Smotkin, *J. Phys. Chem. C*, 2014, **118**, 11711-11722.

27 Y. K. Sun and W. H. Weinberg, *Surf. Sci.*, 1989, **214**, 246-252.

28 M. Lindroos, H. Pfnür, P. Feulner, and D. Menzel, *Surf. Sci.*, 1987, **180**, 237- 251.

29 P. Feulner and D. Menzel, *Surf. Sci.*, 1985, **154**, 465-488.

30 C. H. Mak, J. L. Brand, B. G. Koehler and S. M. George, *Surf. Sci.*, 1987, **191**, 108-120.

31 C. H. Mak, J. L. Brand, B. G. Koehler and S. M. George, *Surf. Sci.*, 1987, **188**, 312-320.

32 I. D. Rosal, L. Truflandier, R. Poteau and I. C. Gerber, *J. Phys. Chem. C*, 2011, **115**, 2169-2178.

33 H. Ueta, I. M. N. Groot, M. A. Gleeson, S. Stolte, G. C. McBane, L. B. F. Juurlink and A. W. Kleyn, *ChemPhysChem.*, 2008, **9**, 2372-2378.

34 I. M. N. Groot, J. C. J. Marcos, C. Díaz, M. F. Somers, R. A. Olsen and G. J. Kroes, *Phys. Chem. Chem. Phys.*, 2010, **12**, 1331-1340.

35 T. Diemant, H. Rauscher, J. Bansmann and R. J. Behm, *Phys. Chem. Chem. Phys.*, 2010, **12**, 9801-9810.

36 K. Reuter and M. Scheffler, *Phys. Rev. B*, 2001, **65**, 035406.

37 K. Reuter and M. Scheffler, *Phys. Rev. B*, 2003, **68**, 045407.

38 G. Kresse and J. Furthmüller, *Comput. Mater. Sci.*, 1996, **6**, 15-50.

39 G. Kresse and J. Furthmüller, *Phys. Rev. B*, 1996, **54**, 11169-11186.

40 P. E. Blochl, *Phys. Rev. B*, 1994, **50**, 17953-17979.

41 G. Kresse, *Phys. Rev. B*, 1999, **59**, 1758-1775.

42 J. P. Perdew, K. Burke and M. Ernzerhof, *Phys. Rev. Lett.*, 1996, **77**, 3865-3868.

43 D. Vanderbilt, *Phys. Rev. B: Condens. Matter Mater. Phys.*, 1990, **41**, 7892-7895.

44 B. Hammer, L. B. Hansen and J. K. Nørskov, *Phys. Rev. B*, 1999, **59**, 7413-7421.

45 S. Grimme, J. Antony, S. Ehrlich and S. Krieg, *J. Chem. Phys.* 2010, **132**, 154104.

46 S. L. Liu, X. X. Tian, T. Wang, X. D. Wen, Y.-W. Li, J. Wang and H. Jiao, *J. Phys. Chem. C* 2014, **118**, 26139-26154.

47 S. L. Liu, X. X. Tian, T. Wang, X. D. Wen, Y.-W. Li, J. Wang and H. Jiao, *Phys. Chem. Chem. Phys.* 2015, **17**, 8811-8821.

48 S. L. Liu, X. X. Tian, T. Wang, X. D. Wen, Y.-W. Li, J. Wang and H. Jiao, *J. Phys. Chem. C* 2015**, 119**, 11714−11724.

49 Y. Shi, Y. Zhu, Y. Yang, Y.-W. Li, and H. Jiao, *ACS Catal.* 2015, **7**, 4020–4032.

50 M. Methfessel and A. T. Paxton, *Phys. Rev. B*, 1989, **40**, 3616-3621.

51 G. Henkelman and H. Jónsson, *J. Chem. Phys.*, 2000, **113**, 9978-9985.

52 Y. Urashima, T. Wakabayashi, T. Masaki and Y. Teresaki, *Mineralogical Journal.*, 1974, **7**, 438-444.

53 W. X. Li, C. Stampfl and M. Scheffler, *Phys. Rev .B*, 2003, **68**, 165412.

54 J. Rogal, K. Reuter and M. Scheffler, *Phys. Rev .B*, 2004, **69**, 075421.

55 F. Zasada, W. Piskorz, S. Cristol, J. F. Paul, A. Kotarba and Z. Sojka, *J. Phys. Chem. C*, 2010, **114**, 22245-22253.

56 T. Wang, X. W. Liu, S. G. Wang, C. F. Huo, Y. W. Li, J. G. Wang and H. Jiao, *J. Phys. Chem. C*, 2011, **115**, 22360-22368.

57 T. Wang, S. G. Wang, Y. W. Li, J. G. Wang and H. J. Jiao, *J. Phys. Chem. C*, 2012, **116**, 6340-6348.

58 T. Wang, X.-X. Tian, Y.-W. Li, J. Wang, M. Beller and H. Jiao, *J. Phys. Chem. C*, 2014, **118**, 1095-1101.

59 T. Wang, X.-X. Tian, Y.-W. Li, J. Wang, M. Beller and H. Jiao, *ACS Catal.*, 2014, **4**, 1991-2005.

60 T. Wang, Y.-W. Li, J. Wang, M. Beller and H. Jiao, *J. Phys. Chem. C*, 2014, **118**, 3162-3171.

61 T. Wang, Q. Luo, Y.-W. Li, J. Wang, M. Beller and H. Jiao, *Appl. Catal. A*, 2014, **478C**, 147-156.

62 O. R. Inderwildi, S. J. Jenkins and D. A. King, *J. Am. Chem. Soc.*, 2007, **129**, 1751-1759.

63 O. R. Inderwildi, S. J. Jenkins and D. A. King, *Angew. Chem. Int. Ed.*, 2008, **47**, 5253-5255.

64 X. Liu, D. R. Salahub, *J. Am. Chem. Soc.,* 2015, **137**, 4249–4259